ACS APPLIED MATERIALS & INTERFACES

www.acsami.org

Research Article

Interaction Dynamics of Liposomal Fatty Acids with Gram-Positive Bacterial Membranes

Sungmin Shin, Dongping Jiang, Jingyeong Yu, Chungmo Yang, Woncheol Jeong, Jian Li, Jieun Bae, Jihoon Shin, Kyongman An, Wooseong Kim, and Nam-Joon Cho*

Cite This: *ACS Appl. Mater. Interfaces* 2025, 17, 23666–23679

Read Online

ACCESS | Metrics & More | Article Recommendations | Supporting Information

ABSTRACT: The increasing prevalence of antibiotic-resistant bacteria has driven the need for alternative therapeutic strategies, with liposomal fatty acids (LipoFAs) emerging as promising candidates due to their potent antibacterial properties. Despite growing interest, the detailed biophysical interactions between LipoFAs and bacterial membranes remain underexplored. In this study, we systematically investigate the mechanistic interactions of liposomal linolenic acid (LipoLNA), linoleic acid (LipoLLA), and oleic acid (LipoOA) with model Gram-positive bacterial membranes using quartz crystal microbalance with dissipation (QCM-D) and fluorescence microscopy. QCM-D analysis revealed that LipoOA displayed the highest rate of membrane fusion, followed by LipoLLA and LipoLNA. Fluorescence microscopy highlighted distinct morphological changes induced by each LipoFA: LipoLNA generated large membrane buds, LipoLLA formed smaller dense protrusions, and LipoOA caused rapid incorporation with uniform dense spots. Furthermore, fluorescence recovery after photobleaching (FRAP) demonstrated that LipoLNA significantly enhanced lipid mobility and membrane fluidity, as confirmed by Laurdan generalized polarization measurements. The extent of unsaturation in LipoFAs was found to play a critical role in their interaction mechanism, with higher degrees of unsaturation inducing greater local curvature stress, increased membrane permeability, and substantial ATP leakage, ultimately leading to improved bactericidal activity. Notably, liposomal formulations exhibited enhanced biocompatibility compared to free fatty acids. These findings provide valuable mechanistic insights into how LipoFAs perturb bacterial membranes, supporting their potential application as alternative antibacterial agents.

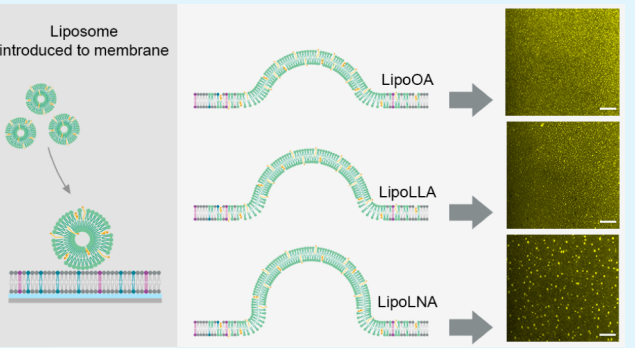

KEYWORDS: *liposomal fatty acids, antibacterial, membrane-active antimicrobial, bacterial membranes, supported lipid bilayer*

INTRODUCTION

Bacterial infections have long posed significant challenges to public health,[1,2] exacerbated by the emergence and rapid dissemination of resistant strains. This escalating threat underscores the urgent need for innovative strategies to combat bacterial infections effectively. Among emerging approaches, fatty acids (FAs) have garnered considerable attention due to their broad-spectrum efficacy against bacterial infections.[3,4] Extensive research has demonstrated that FAs interact with bacterial membranes and possess antibacterial properties.[5−10] Notably, long-chain fatty acids (LCFAs) have drawn wide attention due to their significant antimicrobial activities against Gram-positive bacterial strains.[3,11−13] This interest is driven by their intrinsic antimicrobial properties, widespread availability,[14] and cost-effectiveness.[15,16] However, the practical application of FAs is hindered by challenges such as limited solubility, micelle destabilization,[17] and susceptibility to oxidation.[18,19] Addressing these limitations necessitates the encapsulation of LCFAs with supportive materials to enhance their stability and functionality.

Various strategies have been devised for antibacterial applications using FAs including emulsion,[20,21] liposomes,[22,23] and hydrogels.[24,25] These strategies offer advantages such as higher loading efficiency[26,36] and controlled release[27] of the loaded FAs. Among these carrier systems, liposomes present distinct advantages in facilitating the delivery of amphiphilic antimicrobial agents.[28] This is notably achieved through the process of membrane fusion,[29−31] which significantly enhances the efficacy of FA delivery. Furthermore, liposomes enable the integration of FAs into the membrane structure,[32] altering its properties.

Membrane fluidity is a critical factor in bacterial metabolic processes, including the functioning of membrane-associated

Received: January 23, 2025
Revised: March 18, 2025
Accepted: March 27, 2025
Published: April 14, 2025

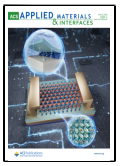

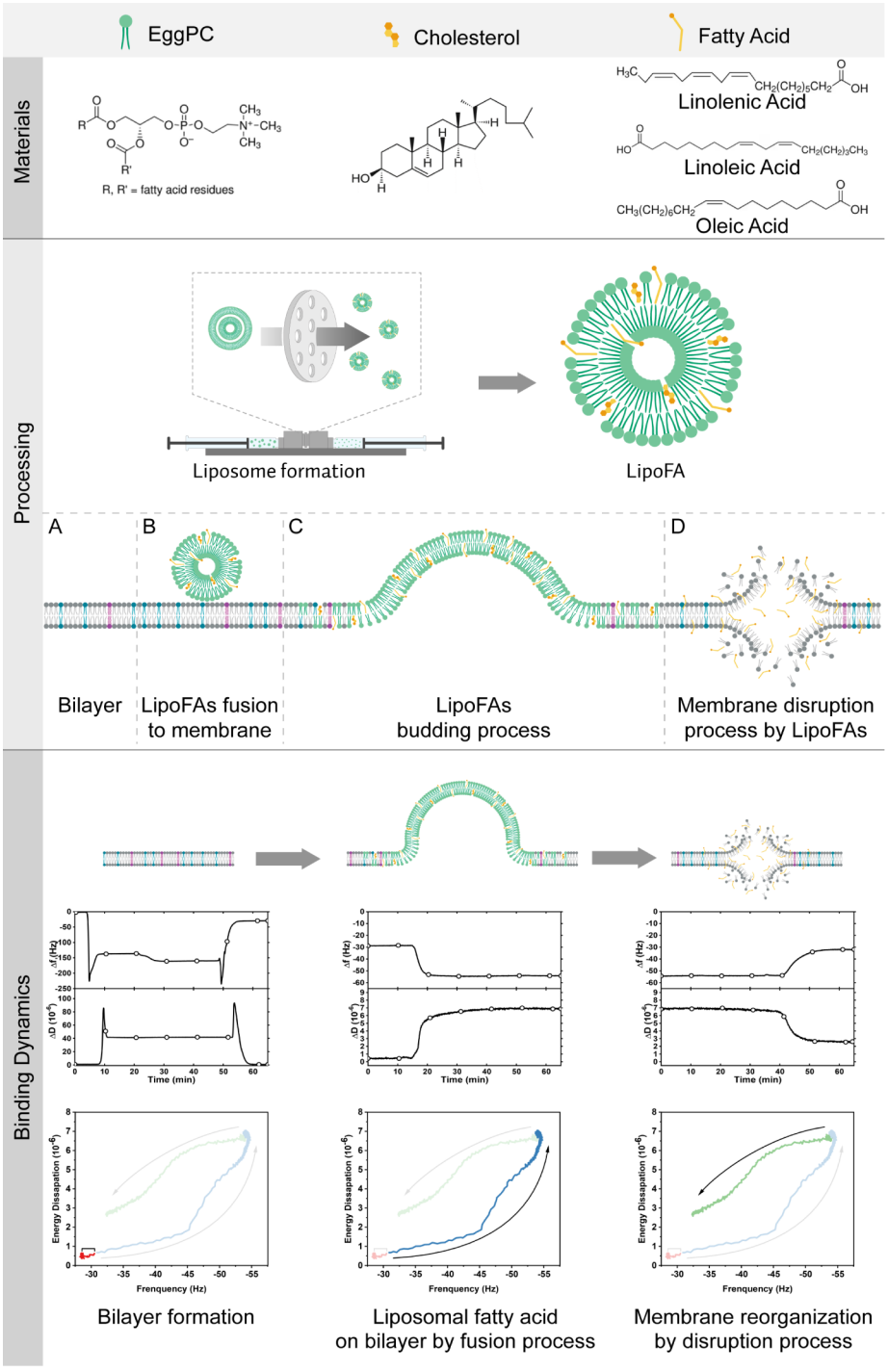

Figure 1. Schematic representation of the experimental approach for developing LipoFAs for antibacterial applications. Liposomes were prepared by hydration of lipid and cholesterol mixtures followed by sonication and extrusion methods. The membrane morphological changes induced by LipoFAs on model bacterial membranes were characterized in the following sequence: (A) bilayer formation, (B) fusion to membrane, (C) budding process, and (D) membrane disruption process. Illustration: Batika Saxena.

proteins,[33] lipid bilayer permeability,[34] and intracellular vesicular transport mechanisms.[35] Membrane fluidity refers to the viscosity of the lipid bilayer in a biological membrane, which affects the lateral mobility of its components, such as lipids and proteins. Insufficient membrane fluidity can disrupt essential cellular processes such as cytokinesis.[436] Another key concept, curvature stress, pertains to the mechanical tension within a membrane caused by deviations from its natural curvature. Such stress influences the structural organization of the membrane and impacts its interactions with external agents, including FAs and liposomes. Alterations in membrane physicochemical properties can compromise the structural integrity necessary for sustaining biological activities.[37] Previous studies have explored the impact of liposomal fatty acids (LipoFAs) on bacteria has been investigated previously. Liposomal oleic acid, for instance, demonstrates rapid fusion with the membrane of *Staphylococcus aureus* MW2, thereby impeding its growth.[29] Similarly, liposomal linolenic acid

https://doi.org/10.1021/acsami.5c00787
ACS Appl. Mater. Interfaces 2025, 17, 23666−23679

exhibits fusion behavior with *Helicobacter pylori*, even when the bacterium is in a dormant state.[38] Additionally, research indicates that FAs can modulate the fluidity of bacterial membranes inhibiting their growth.[39−41] However, the precise biophysical mechanisms underlying the disruption of bacterial membranes by FA-loaded liposomes remain elusive due to the complex nature of biological membranes. Despite promising findings, there is a notable gap in the understanding of how FAs interact with bacterial membranes at a molecular level when delivered via liposomes. Bridging this gap is crucial for optimizing their therapeutic potential against bacterial infections.

Herein, investigations are conducted on the interactions between liposomal linolenic acid (LipoLNA), liposomal linoleic acid (LipoLLA), and liposomal oleic acid (LipoOA) with Gram-positive model membrane using quartz crystal microbalance with dissipation monitoring (QCM-D) and fluorescence microscopy, which offers real-time molecular insights into the kinetics of liposomal fusion, FA adsorption, and membrane responses. These findings elucidate the structural and fluidity changes induced in the model bacterial membrane (Figure 1), along with their correlations to *in vitro* biological activities, offering valuable mechanistic insights into the antibacterial potency and potential clinical applicability of these liposomes in combating bacterial infections.

EXPERIMENTAL SECTION

Reagents. Egg L-α-phosphatidylcholine (Egg PC, cat# 840051), cholesterol (ovine wool, > 98%), 1-palmitoyl-2-oleoyl-*sn*-glycero-3-phospho-(1′-*rac*-glycerol) (POPG), 1,2-dipalmitoyl-*sn*-glycero-3-[phospho-*rac*-(3-lysyl(1-glycerol))] (Lysyl-PG), 1′,3′-bis[1-Palmitoyl-2-oleoyl-*sn*-glycero-3-phospho]-glycerol (Cardiolipin), and 1,2-dioleoyl-*sn*-glycero-3-phosphoethanolamine-*N*-(lissamine rhodamine B sulfonyl) (ammonium salt) (RhB-PE) were obtained from Avanti Polar Lipids, Inc. (Alabaster, AL). Linolenic acid (LNA), linoleic acid (LLA), oleic acid (OA), and 6-Dodecanoyl-*N*,*N*-dimethyl-2-naphthylamine (Laurdan) were procured from Sigma-Aldrich (St. Louis, MO). Tryptic soy broth (TSB), Mueller-Hinton (MH) agar and broth were purchased from Becton Dickinson (Sparks, MD). Phosphate-buffered saline (PBS) was purchased from Gibco (Carlsbad, CA). All solutions were prepared using deionized water treated with a Milli-Q system (>18 MΩ·cm) (Millipore, Billerica, MA).

Preparation and Characterization of Antimicrobial Fatty Acids and Liposomes. LNA, LLA, and OA stock solutions were prepared by dissolving the respective FAs in ethanol at a concentration of 50 mg/mL, with experimental concentrations achieved by dilution with PBS. Liposomes were prepared by the vesicle extrusion technique, incorporating modifications from a previously established protocol.[42,43] LipoLNA, LipoLLA, LipoOA, and BareLipo (bare liposome without added fatty acid) were synthesized by mixing 15 mg of Egg PC, cholesterol, and LNA, LLA, or OA in weight ratios of 5:1:4 and 9:1:0, respectively. These mixtures were combined with 1 mL chloroform and dried using nitrogen at a temperature of 50 °C, followed by overnight storage in a desiccator to remove any residual solvents. The dried lipid film was then hydrated with 3 mL sterile PBS buffer (pH 7.5). The resulting lipid suspension was vortexed for 15 s, sonicated in a bath sonicator (RS PRO, Kuala Lumpur, Malaysia), and then further sonicated using a 20 kHz ultrasonic probe with a 12 mm tip diameter (QSonica, Newton, CT) at 20 kHz, 500 W, and 40% amplitude for 5 min to produce small unilamellar vesicles (SUVs). These final vesicles were then extruded through a polycarbonate membrane with 400 nm-sized polycarbonate (PC) membranes, followed by further extrusion through a 100 nm sized pores 21 times using a mini-extruder (Avanti Polar Lipids Inc., Alabaster, AL). The hydrodynamic size and surface zeta potential of LipoLNA, LipoLLA, LipoOA, and BareLipo were analyzed using dynamic light scattering (DLS) and zeta PALS analyzer (Brookhaven Instruments, Holtsville, NY). BareLipo was utilized as a negative control and all experimental characterization tests were conducted in triplicate at room temperature.

Cryogenic Electron Microscopy (Cryo-EM) Imaging. For Cryo-EM imaging, samples were prepared by placing 3 μL of the sample onto a 400-mesh Tedpella lacey carbon copper grid, which was coated with ultrathin carbon film (Ted Pella, Inc.) and glow-discharged in air for 60 s. Subsequently, the grid was blotted for either 1 or 2 s (blot force 1) at a temperature of 22 °C and 100% humidity before being immersed in liquid ethane using an FEI Vitrobot Mark IV. Micrographs were acquired using a 300 kV Titan Krios cryo-transmission electron microscope, equipped with a Selectris X imaging filter and a Falcon 4i direct electron detector. Images were acquired at 53,000× magnification within a pixel size of 2.4 Å/px.

Lipid Preparation for Supported Lipid Bilayer (SLB) Formation. A Gram-positive lipid membrane consisting of anionic lipid 1-palmitoyl-2-oleoyl-*sn*-glycero-3-phospho-(1′-*rac*-glycerol) (POPG), cationic lipid 1,2-dipalmitoyl-*sn*-glycero-3-[phospho-*rac*-(3-lysyl(1-glycerol))] (Lysyl PG), and anionic lipid 1′,3′-bis[1-Palmitoyl-2-oleoyl-*sn*-glycero-3-phospho]-glycerol (CL) was mixed in chloroform to achieve a total concentration of 0.3 mg/mL as reported in our previous work.[44] Lipid mixture was dried under nitrogen gas flow to obtain dried lipid films that were desiccated using nitrogen and vacuum-stored overnight to confirm elimination of the organic solvent. To enhance solubility, the anionic and cationic lipids were dissolved in ethanol at 70 °C for 1−2 min to achieve a concentration of 1 mg/mL. Prior to each experiment, this solution was further diluted in isopropanol.

Quartz Crystal Microbalance with Dissipation (QCM-D) Experiments. To examine the molecular level interaction between the liposomes and SLBs, QCM-D experiments were conducted using a four-channel Q-Sense E4 instrument (Q-Sense AB, Gothenburg, Sweden). The QCM-D technique measures changes in the frequency (Δf) and energy dissipation (ΔD) of an oscillating piezoelectric quartz crystal sensor chip over time. These measurement signals provide mechanistic insights into the changes in mass and dissipation properties of the adsorbed film. Five MHz sensor chips, coated with silicon dioxide (model no. QSX 303, Biolin Scientific), were used. Prior to each experiment, the chips were washed with 1% SDS, DI water, and ethanol. Subsequently, the chips were dried with nitrogen gas and treated with oxygen plasma for 1 min using an Expanded Plasma Cleaner (PDC-002, Harrick Plasma, Ithaca, NY). Bacterial model membrane SLBs were formed using the solvent-assisted lipid bilayer (SALB) technique.[45] Each SLB was used only once per experiment. Initially, a baseline signal was recorded in an aqueous buffer solution (10 mM Tris, 150 mM NaCl, pH 7.5). The buffer solution was then replaced with an isopropanol solution, followed by the addition of 0.3 mg/mL Gram-positive membrane lipids in isopropanol solution. Subsequently, the solvent was exchanged with PBS to form the SLB. Once bilayer formation was complete, test liposome samples at concentrations of 500 μg/mL and 15.625 μg/mL in PBS solution were introduced, followed by a final PBS rinse. All liquid samples were introduced into the measurement chamber using a peristaltic pump (Reglo Digital, Ismatec, Glattbrugg, Switzerland) at a flow rate of 50 μL/min. The temperature was maintained at room temperature (25.0 ± 0.5 °C) throughout the experiments. Data collection was performed at the third (n = 3), fifth (n = 5), seventh (n = 7), and ninth (n = 9) overtones using the Q-Soft software program (Biolin Scientific). The presented data were specifically obtained at the fifth overtone, and all data processing was completed using the Q-Tools (Biolin Scientific) and OriginPro (OriginLab, Northampton, MA) software programs.

Time-Lapse Fluorescence Microscopy. Epifluorescence microscopy was employed to visually monitor surface membrane morphological changes in SLBs on silica dioxide substrates treated with LipoLNA, LipoLLA, LipoOA, and BareLipo. These experiments were conducted using an Eclipse TI-E inverted microscope (Nikon, Tokyo, Japan) equipped with a 60× magnification (NA = 1.49) oil-immersion objective lens (Nikon). Micrographs were captured using an iXon EMCCD camera (Andor Technology, Belfast, Northern

https://doi.org/10.1021/acsami.5c00787
ACS Appl. Mater. Interfaces 2025, 17, 23666−23679

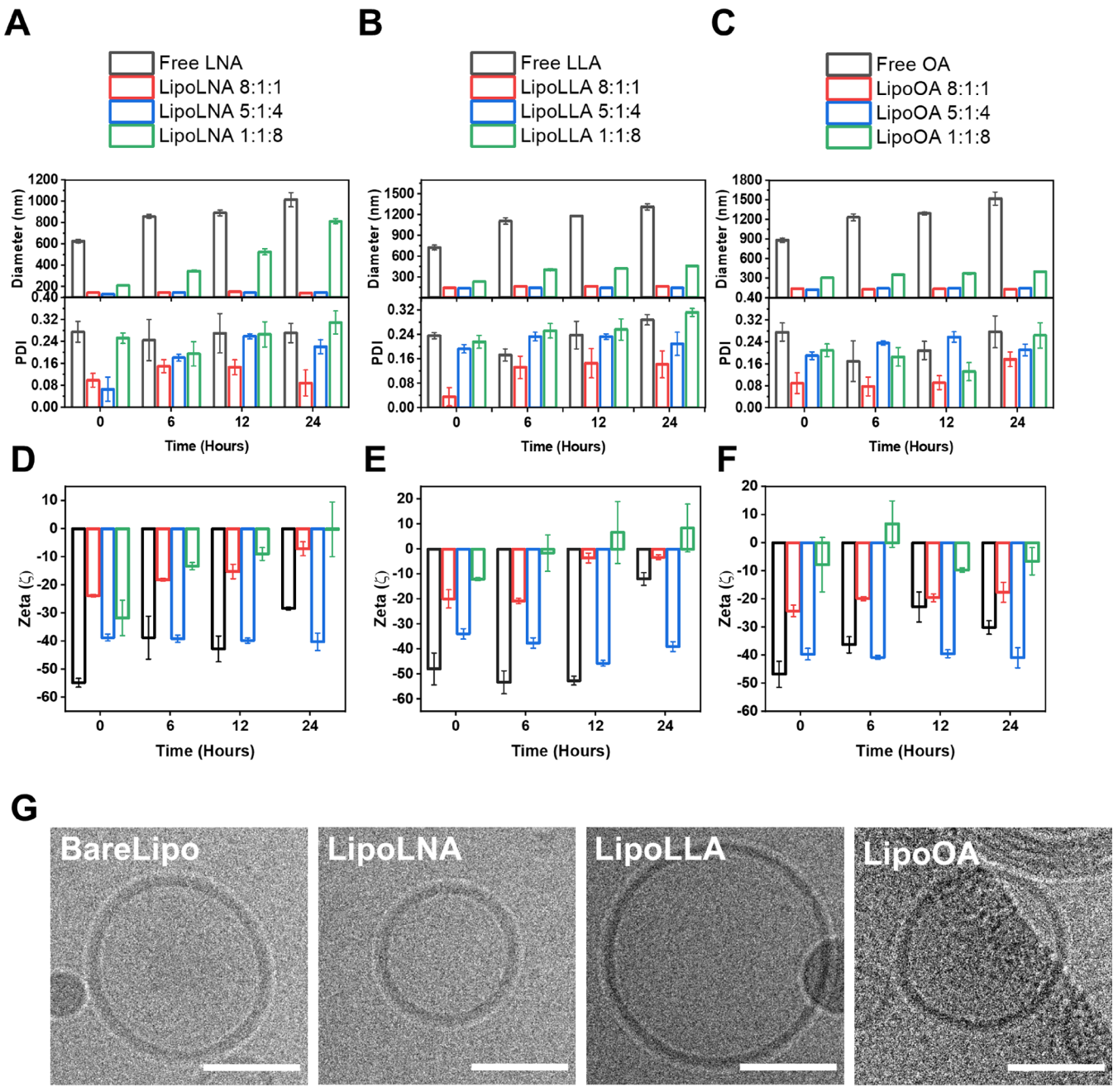

Figure 2. Characterization of LipoFAs. (A–C) Change in hydrodynamic size (diameter, nm) and PDI of FFAs and LipoFAs with different compositions measured by DLS. (D–F) Change in surface zeta potential (mV) of FFAs and LipoFAs with different compositions measured by DLS over 24 h (n = 3, mean ± SD). (G) Representative cryo-EM images of (1) BareLipo, (2) LipoLNA, (3) LipoLLA, and (4) LipoOA (Scale bar: 50 nm).

Ireland) featuring a resolution with 512 pixel × 512 pixel and a pixel size of 0.267 × 0.267 μm^2. Illumination was provided by a fiber-coupled mercury lamp (Intensilight C-HGFIE, Nikon) and a TRITC filter to excite the fluorescently labeled bacterial phospholipids. SLBs were fabricated on a glass coverslip as a substrate contained within a flow-through chamber (sticky slide VI 0.4, Ibidi, Germany) using the SALB method.[45−47] Following SLB formation, the chamber was rinsed with PBS buffer solution, and the prepared LipoLNA, LipoLLA, LipoOA, and BareLipo was introduced at a flow rate of 50 μL/min. Micrographs were taken every 5 s for 1 h at room temperature to examine the time-dependence of the effect of the LipoFAs on the SLBs. t = 0 s was designated as the starting time of test sampleinjection. The collected images were analyzed using ImageJ (National Institutes of Health, Bethesda, MD, USA).

Measurements of Fluorescence Recovery after Photobleaching (FRAP). FRAP techniques were used to evaluate the lateral diffusivity of SLBs labeled with Rhodamine-PE lipids before and after exposure to LipoFAs. Photobleaching process was performed using a 532 nm, 100 mW laser (Klastech Laser Technologies, Dortmund, Germany) to generate circular spots with a 20-μm diameter for 5 s. Fluorescence micrographs were taken every 2 s over 120 s to track fluorescence recovery. The lateral diffusion coefficients were computed from the FRAP data using a Hankel transform method[48] implemented in Matlab (MathWorks, USA).

Membrane Fluidity Assay. An overnight culture of *S. aureus* MW2 was diluted 1:100 in 2 mL TSB and incubated at 37 °C until OD_{600} = 1.0. The bacteria were then coincubated with 10 μM Laurdan in the dark for 10 min. After staining, the bacterial

https://doi.org/10.1021/acsami.5c00787
ACS Appl. Mater. Interfaces 2025, 17, 23666−23679

suspension was washed four times with PBS and concentrated 2-fold. This concentrated bacterial suspension was mixed with equal volumes of PBS, benzyl alcohol (BA), BareLipo, LipoLNA, LipoLLA, and LipoOA at twice the desired concentrations. Following a 1 h incubation in the dark at room temperature, the fluorescence intensity of Laurdan was evaluated at emission wavelengths of 435 nm 490 nm, upon excitation at 350 nm, using a spectrophotometer (Tecan Spark, Tecan, Zurich, Switzerland). Membrane fluidity was quantified by the Laurdan generalized polarization (GP) index, which is expressed as $GP = (I_{435} - I_{490})/(I_{435} + I_{490})$. Benzyl alcohol at a concentration of 50 mM was use as a positive control.

Liposome Fusion with *S. Aureus* MW2. The fusion between LipoLNA, LipoLLA, LipoOA and *S. aureus* MW2 was studied using a fluorescence method. DMPE-RhB (0.5 mol %) was mixed with EggPC, cholesterol, and FFA to prepare fluorescently labeled LipoLNA, LipoLLA, and LipoOA. Subsequently, 1 mL of the LipoFA suspension was mixed with 1.5×10^8 CFU/mL *S. aureus* MW2. After a 30 min incubation, the bacteria were collected by centrifugation at 17,500 × g for 5 min and fixed with 2% (v/v) glutaraldehyde in PBS at room temperature for 20 min. The bacteria were washed and resuspended in 500 μL DI water. For imaging purposes, 10 μL of the bacterial suspension was mixed with 10 μL DAPI-containing mounting media (Fluoroshield with DAPI, Sigma-Aldrich) and placed on a glass slide. The sample was imaged using a 63× oil immersion objective on a Zeiss Observer II. The experiments were performed independently three times unless otherwise specified. Statistical analysis was performed using a two-tailed *t* test using Microsoft Excel (Microsoft, Redmond, WA, USA), with correlations having a p-value <0.05 considered statistically significant ($*p < 0.05$, $**p < 0.01$, and $***p < 0.001$).

Time-Kill Kinetics Assessment. An overnight culture of *Staphylococcus aureus* MW2 was diluted 1:10,000 in 25 mL of tryptic soy broth (TSB) and incubated at 37 °C with shaking at 200 rpm until the OD_{600} reached 0.05. The logarithmic-phase cells were then washed three times with PBS and adjusted to an OD_{600} of 0.05. The culture was then mixed with an equal volume of prewarmed TSB containing twice the target concentration of the prepared LipoFAs and BareLipo, then distributed into a 96-well analysis block (Bioneer cat# 90063, Daejeon, South Korea). The analysis block was incubated at 37 °C with shaking at 450 rpm. Samples were collected hourly, serially diluted 10-fold in PBS, and streaked onto cation-adjusted Mueller-Hinton (CaMH, BD cat# 212322) agar. After overnight incubation at 37 °C, colony counts were determined to assess the number of surviving cells. The experiment was performed in triplicate.

Assessment of Membrane Integrity. Membrane permeability in MRSA induced by LipoFAs was evaluated using SYTOX Green dye (ThermoFisher cat# S7020), which binds to DNA but does not penetrate intact cell membranes. *S. aureus* MW2 cells were washed three times with PBS and adjusted to an OD_{600} of 0.4. SYTOX Green was added to the cell suspension to a final concentration of 5 μM, followed by incubation in the dark at room temperature for 30 min. After incubation, 50 μL of the SYTOX Green-bacterial mixture was added to each well of a black, clear-bottom 96-well plate (Greiner Bio-One Cat no. 665090) containing LipoFA compounds at concentrations ranging from 16 μg/mL to 500 μg/mL. Fluorescence measurements were taken at room temperature over the course of 1 h using a BioTek Cytation 5 multimode reader (BioTek, USA), with excitation and emission wavelengths set at 485 and 525 nm, respectively. The experiment was conducted in triplicate.

Extracellular ATP Leakage Measurement. Extracellular ATP leakage from *S. aureus* MW2 cells was assessed using the RealTime-Glo Extracellular ATP Assay (Promega, Madison, WI, USA). Logarithmic-phase *S. aureus* MW2 cells were washed three times with PBS and adjusted to an OD_{600} of 0.4. The ATP assay reagent mixture was prepared at a 4x concentration following the manufacturer's instructions. The prepared LipoFAs and BareLipo were serially diluted to concentrations ranging from 16 μg/mL to 500 μg/mL in a black, clear-bottom 96-well plate (Greiner Bio-One Cat no. 665090). Each well was then supplemented with 50 μL of the reagent mixture and 50 μL of the bacterial suspension. The plate was incubated statically at 37 °C for 20 min. After incubation, an additional 33.4 μL of the 4x reagent mixture was added to each well, and luminescence was measured using a BioTek Cytation 5 multimode reader. All experiments were conducted in triplicate.

Cell Viability Testing. The impact of LipoLNA, LipoLLA, LipoOA, and BareLipo on cell viability was evaluated by measuring dehydrogenase activity in mouse fibroblast cells (L-929) (ATCC, USA) and human keratinocyte cells (HaCat) (CLS Cell Lines Service, Eppelheim, Germany). The cell viability was evaluated using the cell counting kit-8 (CCK-8) (Dojindo Molecular Technologies, Rockville, MD). L-929 and HaCat cells were cultured in Dulbecco's modified eagle medium (DMEM) supplemented with 10% fetal bovine serum (Gibco) and 1% penicillin-streptomycin (Hyclone) in a humidified 5% CO_2 incubator at 37 °C. L-292 cells were seeded at a density of 5×10^3 cells per well, and HaCaT cells at a density of 1×10^4 cells per well, in 96-well tissue culture plates. After 24 h incubation, experimental samples ranging from 8 μg/mL to 128 μg/mL were added, and the cells were further incubated under the same conditions for an additional 24 h. Following treatment, the cells were incubated in 10% CCK-8 solution containing water-soluble tetrazolium salt (WST-8) for 2 h. Cell viability was determined by measuring sample absorbance at a wavelength of 450 nm using a microplate reader (Tecan Spark, Tecan, Zurich, Switzerland). All experiments were performed three times each.

RESULTS AND DISCUSSION

Preparation and *In Vitro* Characterization of LipoFAs. The stability of the prepared LipoFAs and FFA micelles was evaluated by monitoring changes in size and zeta potential over 24 h using dynamic light scattering (DLS). Figure 2A–F depict the size changes of FFAs and LipoFAs at a concentration of 5 mg/mL in PBS buffer, with samples diluted 10-fold for zeta potential measurements. All FFAs demonstrated a significant increase in size over 24 h. For instance, the measured size of LNA increased from 626 ± 18 nm to 1016 ± 67 nm, LLA increased from 728 ± 35 nm to 1314 ± 45 nm, and OA increased from 885 ± 34 nm to 1523 ± 10 nm, indicating rapid aggregation of FFAs. Similarly, the size of LipoFAs loaded with 80% FAs (weight ratio of 1:1:8) also increased markedly overnight, with LipoLNA growing from 213 ± 4 nm to 813 ± 24 nm, LipoLLA growing from 236 ± 5 nm to 461 ± 11 nm, and LipoOA growing from 308.7 ± 9 nm to 404 ± 9 nm. This increase in final liposome sizes was attributed to the structural changes in FAs, with OA showing denser packing with phospholipids than LNA.[49] In contrast, LipoFAs with weight ratios of 8:1:1 and 5:1:4 displayed better stability, maintaining their sizes within 150 nm over 24 h. The polydispersity indices (PDIs) of FFAs and their corresponding LipoFAs with a weight ratio of 1:1:8 exceeded 0.3 over a 24 h period, whereas the PDIs for LipoFAs with weight ratios of 8:1:1 and 5:1:4 remained below 0.24. This suggests that an excess of FAs results in unstable liposomes.[50] Additionally, the PDIs of the prepared LipoFAs slightly increased overnight, with higher PDIs observed in the less stable groups (Figure 2A–C).

The zeta potential of the FFAs and LipoFAs was measured at 0, 6, 12, and 24 h. It was observed that only liposomes with a weight ratio of 5:1:4 exhibited consistent and stable trends in line with their zeta potential stability (Figure 2D–F).[51] Zeta potential, indicative of the effective electric charge on liposome surface, is used to determine the stability and aggregation behavior of liposomal formulations.[52] This parameter serves as an indicator of the colloidal stability of liposomes, with higher absolute values suggesting enhanced particle stability.[53] For LipoFAs with a weight ratio of 5:1:4, the surface zeta potential was measured as −39 ± 1 mV for LipoLNA, −34 ± 2 mV for

https://doi.org/10.1021/acsami.5c00787
ACS Appl. Mater. Interfaces 2025, 17, 23666−23679

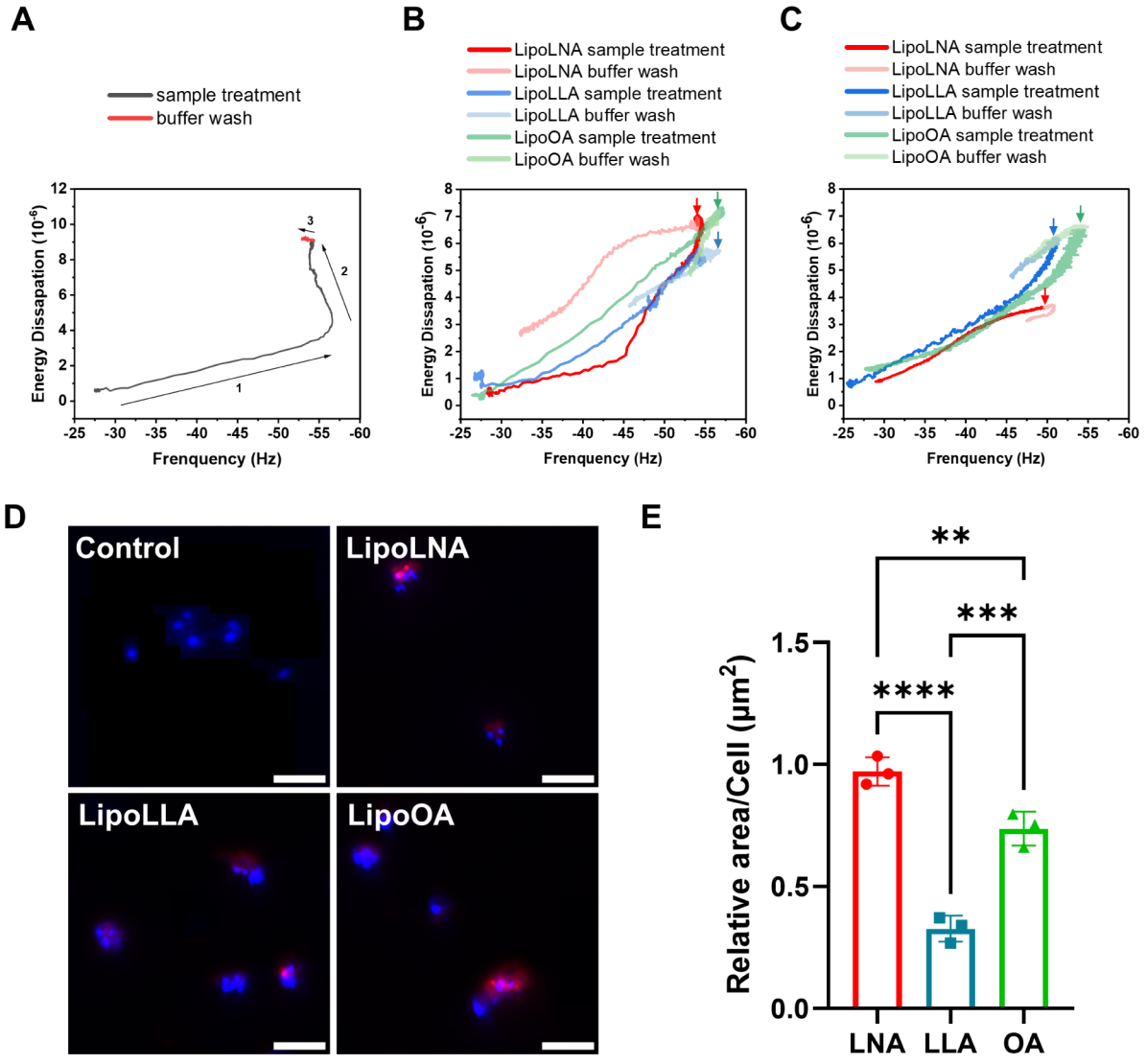

Figure 3. Biophysical characterization of membrane interaction and fusion with *S. aureus* MW2. Viscoelastic fingerprints of interactions of LipoFAs with model Gram-positive bacterial SLBs. Frequency-dissipation (F-D) curves for (A) BareLipo, (B) 500 μg/mL LipoFAs, and (C) 15.625 μg/mL LipoFAs. Arrows in panel (A) indicate stages of the interaction, while the downward arrow in panels B and C marks the initiation of buffer washing. (D) Fluorescence images of the fusion activity between RhB-labeled LipoFAs (red) and DAPI-stained bacteria (blue). (E) Analysis of fusion contact area quantified by RhB-conjugate liposome. The value for Control group was 0. p values of <0.05 were considered statistically significant (*p < 0.05, **p < 0.01, and ***p < 0.001). Control bacteria were incubated with PBS (Scale bar: 5 μm).

LipoLLA, −40 ± 2 mV for LipoOA, and −4 ± 0.4 mV for BareLipo. The marked decrease in surface zeta potential suggests the integration of FAs into the lipid layers, with the carboxylic acid group deprotonating to COO^- at neutral pH.[54] Liposomes with diameters less than 50 nm exhibit significant instability and a tendency to fuse due to high surface tension.[29] Conversely, larger liposomes (>200 nm) tend to be stable but face penetration challenges.[55,56] Intermediate-sized liposomes (50−200 nm) offer relatively good stability, fusion capability, and penetration efficiency.[29] Therefore, the 5:1:4 weight ratio was selected due to its moderate size (~140 nm) and physical stability. The size and shape of the prepared liposomes were further validated through cryogenic-electron microscopy (cryo-EM) (Figure 2G), revealing both BareLipo and LipoFAs as spherical with clear single or double layers, approximately 100 nm in size. The difference in sizes between cryo-EM and DLS may be due to the surface ions that provides a larger dynamic diameter.[57]

Frequency and Dissipation Relations (F-D Curves) for LipoFAs on Gram-Positive Model Membranes. The frequency and dissipation relations for LipoFAs with model membrane were derived from the QCM-D analysis (Figure S1), allowing for real-time tracking of variations in the membrane's mass and viscoelastic properties (Figure 3A−C).

In Figure 3A, the initial introduction of BareLipo to the model membrane surface resulted in adhesion,[58,59] evidenced by a decrease in frequency and an increase in dissipation [-f, +D]. This stage indicates the initial adsorption of liposomes onto the membrane surface. In the second stage, a continued increase in dissipation and a slight increase in frequency [+f, +D] were observed, suggesting the incorporation of lipid molecules within the model membrane.[60,61] During buffer washing in stage 3, both frequency and dissipation remained relatively unchanged, indicating that fusion of BareLipo with the membrane had occurred. Overall, the higher dissipation

https://doi.org/10.1021/acsami.5c00787
ACS Appl. Mater. Interfaces 2025, 17, 23666−23679

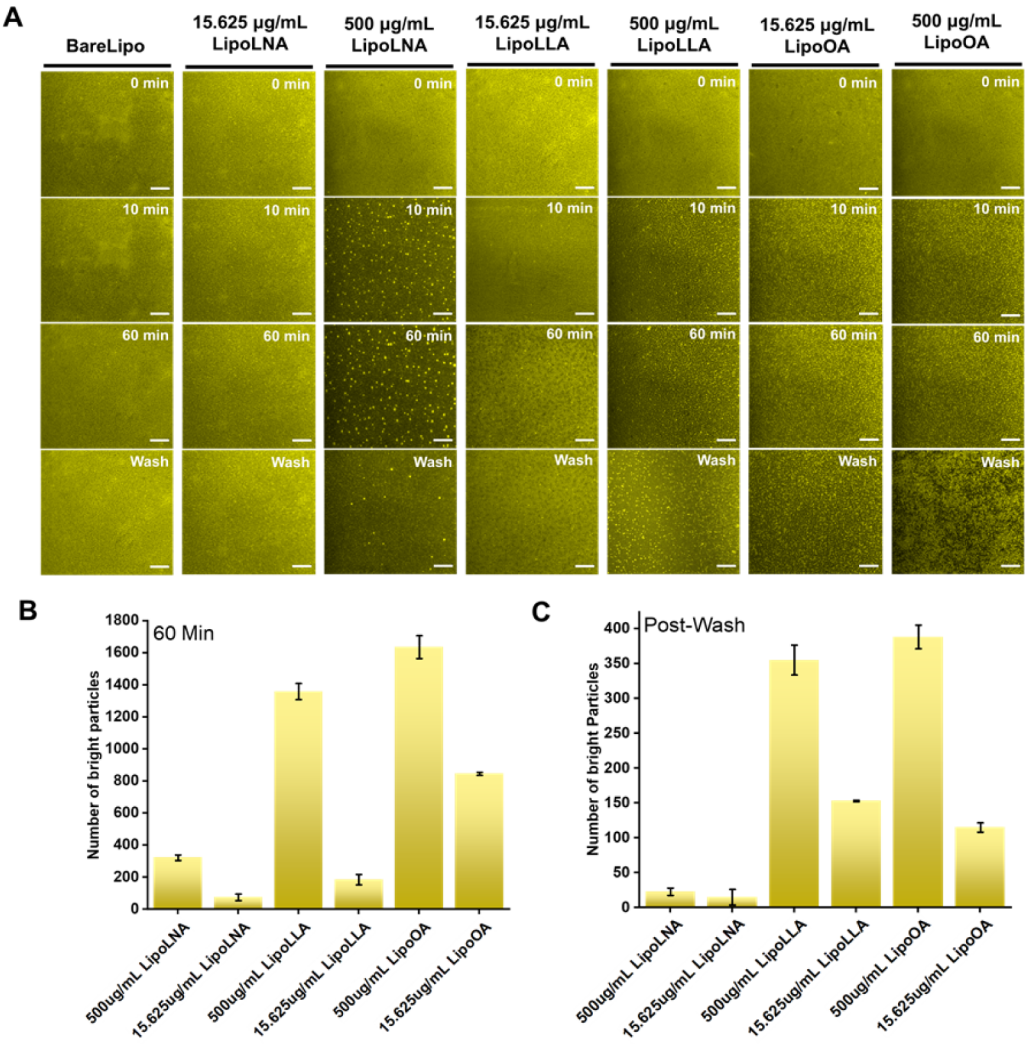

Figure 4. Quantitative analysis of bright spot formation in Gram-positive model membranes. Time-lapse microscopic observation of membrane morphological responses in SLBs induced by BareLipo, LipoOA, LipoLLA, and LipoLNA. (A) Sequential image snapshots depicting the morphological changes of SLBs upon interaction with BareLipo and LipoFAs at varying concentrations (Scale bar: 20 μm). The total number of high-intensity points (B) after sample treatment and (C) postwashing (n = 5, mean ± SD). The numbers were calculated using ImageJ.

values demonstrated that the phospholipids changed the viscoelastic properties of the membrane.

The frequency and dissipation relations for LipoLNA, LipoLLA, and LipoOA are shown in Figure 3B. Similar to the observations in stage 1 of BareLipo, the initial decrease in frequency indicates the adhesion of LipoFAs to the Gram-positive model membrane, characterized by the shift [-f, + D]. Variations in the $\partial D/\partial f$ ratio among LipoLNA, LipoLLA, and LipoOA were primarily due to differences in the rate of dissipation increase. LipoOA exhibited the highest $\partial D/\partial f$ values, suggesting a higher degree of incorporation into the model membrane (Figure 3B), as the viscoelasticity of the membrane increased most rapidly. Furthermore, the consistent $\partial D/\partial f$ ratio for LipoOA indicated that fusion began upon adsorption onto the model membrane. LipoLLA showed a slight increase in the $\partial D/\partial f$ ratio, indicative of a small impediment in liposome fusion and a slower fusion rate compared to LipoOA. Conversely, LipoLNA exhibited a noticeable change in the $\partial D/\partial f$ ratio. The initial $\partial D/\partial f$ ratio for LipoLNA (Figure 3B) suggests slower incorporation into the model membrane, followed by a significant increase in the $\partial D/\partial f$ ratio, corresponding to a faster rise in dissipation for this sample. This may be attributed to the larger tail volume of LNA, which could impede the fusion rate.[62,63] After rinsing with buffer at t = 100 min, the end points in the f-D curves provided insights of the membrane property changes. In Figure 3C, the frequency changes of LipoFAs after buffer rinsing were −21.9 ± 0.1 Hz for LipoLNA, −8.6 ± 0.0 Hz for LipoLLA, and −3.4 ± 0.1 Hz for LipoOA, indicating a decreasing trend in mass loss and suggesting more incorporation with the membrane components.

The membrane interactions were less pronounced at a lower concentration of 15.625 μg/mL (Figure 3C), indicating the concentration-related effects of LCFAs. The adhesion process was less significant due to the lower sample concentration. Given the absence of notable variations in the surface zeta potential of LipoFAs, they should present a similar adsorption ability resulting in similar frequency measurement responses. f Interestingly, the frequency end points before buffer rinsing were −49.7 ± 0.1 Hz for LipoLNA, −51.2 ± 0.0 Hz for LipoLLA, and −54.0 ± 0.2 Hz for LipoOA, respectively, demonstrating an increase in mass and indicating a stronger incorporation capability of OA into the model membrane. Less change in mass was observed compared to higher LipoFA

https://doi.org/10.1021/acsami.5c00787
ACS Appl. Mater. Interfaces 2025, 17, 23666−23679

A

	diffusion coefficient ($\mu m^2/s$)			
	before treatment	after treatment		mobile fraction
BareLipo	0.44 ± 0.04	0.59 ± 0.11	+35.2%	87.0 ± 1%
500 μg/mL LipoLNA	0.46 ± 0.04	0.54 ± 0.03	+18.4%	80.0 ± 3%
500 μg/mL LipoLLA	0.45 ± 0.03	0.28 ± 0.02	-37.8%	43.8 ± 0.8%
500 μg/mL LipoOA	0.49 ± 0.04	0.04 ± 0.02	-91.8%	25.7 ± 2.2%

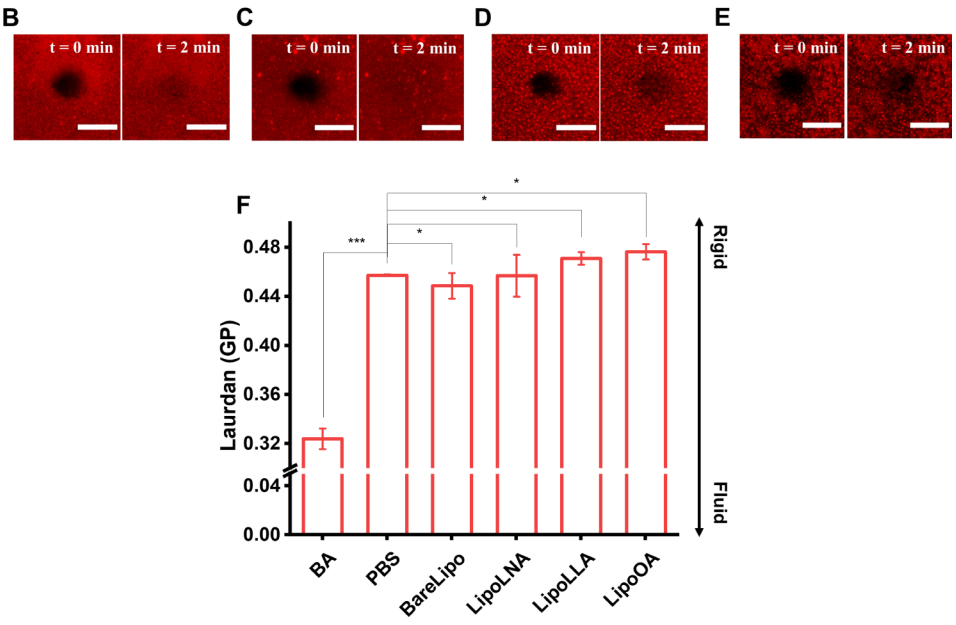

Figure 5. Membrane fluidity changes induced by LipoFAs on Gram-positive model membranes and *in vitro* bacterial fusion assays. (A) Summary of diffusion coefficients and mobile fractions for the Gram-positive model membrane before and after treatment with LipoFAs. Fluorescence micrographs at 0 and 2 min after photobleaching for model membranes treated with (B) BareLipo, (C) LipoLNA, (D) LipoLLA, and (E) LipoOA (Scale bar: 20 μm). (F) Membrane fluidity of *S. aureus* MW2 treated with LipoFAs and BareLipo for 1 h. Laurdan GP index = $(I_{435} - I_{490})/(I_{435} + I_{490})$, where 435 and 490 are the emission intensities at 435 and 490 nm, respectively, when excited at 350 nm (n = 3, mean ± SD). Statistical significance was determined with p values <0.05 as significant (*p < 0.05, **p < 0.01, and ***p < 0.001).

concentrations after buffer washing, while the final dissipation for LipoOA was the highest, primarily due to the greater incorporation of OA into the model membrane, resulting in the membrane instability.

To verify the fusion behaviors of LipoFAs, *in vitro* interactions between LipoFAs labeled with lipophilic RhB-PE fluorophore and *S. aureus* MW2 were investigated (Figure 3D). The bacteria were stained with DAPI (blue), and only DAPI fluorescence was observed in PBS buffer solution. In contrast, when the bacteria were incubated with RhB-PE labeled LipoFAs, distinct RhB red fluorescence signal was observed around the bacteria, confirming fusion with bacteria. Therefore, the fluorescence images are consistent with our QCM-D analysis.

Quantitative Analysis of Morphological Changes on Gram-Positive Model Membranes. To verify the f-D relation signatures and their corresponding kinetic effects on membrane morphology, fluorescence microscopy was employed to investigate and monitor the direct interactions between LipoFAs and Gram-positive model membranes. These membranes were formed using the solvent-assisted lipid bilayer (SALB) method, following the protocol detailed in the experimental section. Freshly prepared LipoFAs were introduced to the formed lipid bilayers, with the introduction time marked as t = 0 min. Concentrations of 500 μg/mL and 15.625 μg/mL were selected for evaluation.

LipoLNA on Gram-Positive Bacterial Membranes. The interaction of LipoLNA with the Gram-positive model membrane is presented in Figure 4A. Upon exposure to 500 μg/mL LipoLNA, rapid morphological changes were observed due to the increased local curvature stress on membrane caused by the insertion of FAs.[64] Large dots with high fluorescence intensity appeared 10 min after sample introduction, with a total count number of 322 ± 17 dots. The emergence of fluorescent dots on the membrane suggests morphological alterations that lead to an increased density of fluorescent lipids, a phenomenon induced by the stress associated with the incorporation of FAs, suggesting the increased curvature stress induced by the incorporation of LNA into the bacterial membrane.[65] This increased stress restricts the rearrangement of lipid molecules, as it results from the higher degree of tail unsaturation and the higher packing parameter of LNA, both of which promote greater membrane curvature and protrusions. After rinsing with buffer, a significant reduction in the spots was observed, with only 23 ± 5 dots remaining, suggesting the removal of the formed structures. In contrast, a 15.625 μg/mL concentration of LipoLNA elicited negligible morphological response, with no significant disturbance observed on the model membrane.

https://doi.org/10.1021/acsami.5c00787
ACS Appl. Mater. Interfaces 2025, 17, 23666−23679

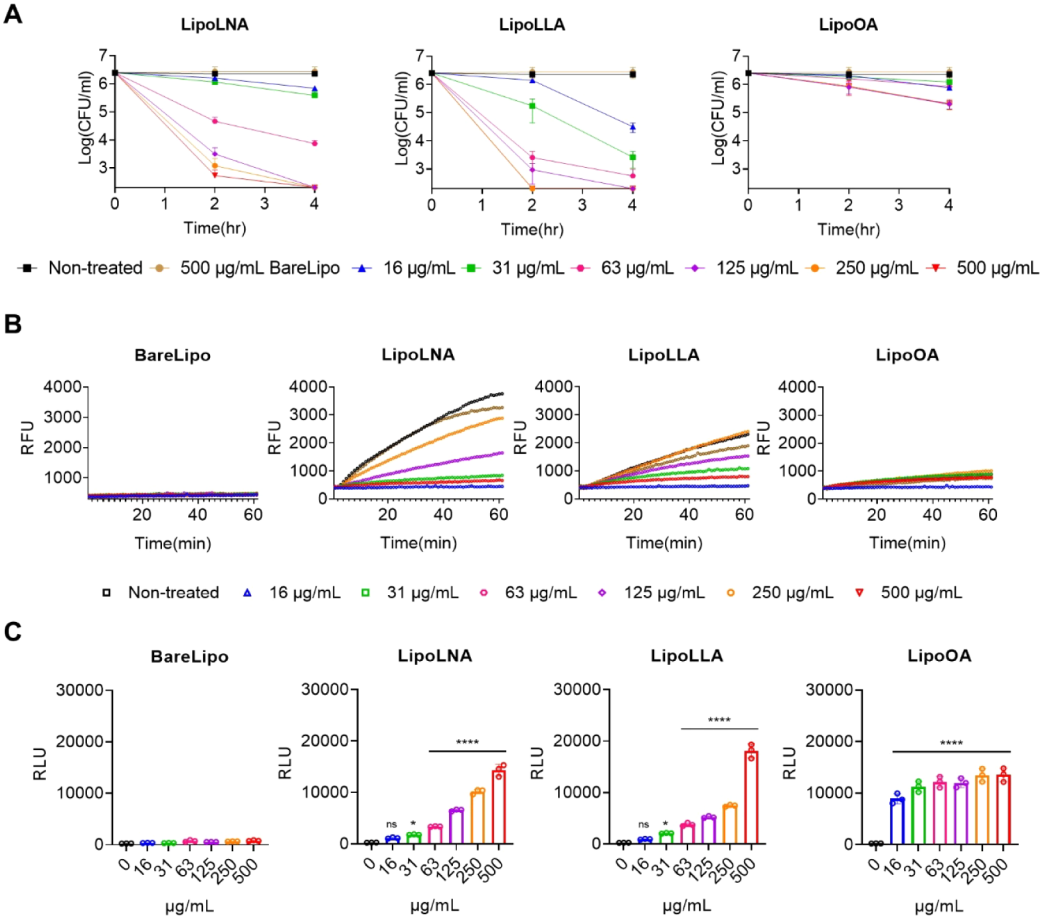

Figure 6. Bactericidal effects of lipophilic liposomal fatty acids (LipoFAs) against *Staphylococcus aureus* MW2 and their impact on the bacterial membrane integrity. (A) Exponential-phase *S. aureus* MW2 cells were treated with LipoFAs for 4 h, with bacterial viability assessed at 2 h intervals. The detection limit was set at 2×10^2 CFU/mL, with error bars representing the standard deviation (SD) from biological triplicates. (B) Membrane permeability of actively growing *S. aureus* MW2 cells following LipoFAs treatment was evaluated using SYTOX Green. Data represent the average of three independent experiments. (C) ATP leakage from growing MRSA cells treated with LipoFAs for 10 min was evaluated using an ATP luminescence assay. Individual data points are shown, with error bars representing the mean ± standard deviation (SD) ($n = 3$). Statistical differences were analyzed by one-way ANOVA followed by Tukey's post hoc test (* $p < 0.1$, **** $p < 0.0001$).

LipoLLA on Gram-Positive Bacterial Membranes. Figure 4A illustrates the real-time monitoring of interactions between the model membrane and LipoLLA. When exposed to 500 μg/mL of LipoLLA, minor morphological changes were observed, evidenced by the presence of 1359 ± 50 small dots. The emergence of smaller and denser spots following LipoLLA introduction indicates increased incorporation and rearrangement of lipid molecules within the model membrane, accompanied by the formation of flatter bud structures. These morphological changes are consistent with the higher $\partial D/\partial f$ ratio compared to LipoLNA, as shown in Figure 3B, which suggests a higher fusion rate and incorporation efficiency. After buffer rinsing, the number of bright dots significantly reduced to 355 ± 21 with a 73.8% removal rate. The remaining dots exhibited greater aggregation, implying a rearrangement of the membrane lipid molecules. This is supported by the decreased dissipation leading to a more rigid system. Conversely, introducing a lower concentration of LipoLLA resulted in minimal interactions with the model membrane. Nevertheless, the presence of small dark regions suggests some degree of fusion with the model membrane.

LipoOA on Gram-Positive Bacterial Membranes. LipoOA rapidly induced the formation of numerous small and dense spot protrusions on the model membrane, indicating effective fusion and incorporation of its components. The presence of these dense spots indicated rapid fusion and rearrangement with the model membrane, resulting in higher $\partial D/\partial f$ ratios after sample treatment (Figure 3B). A total of 1636 ± 71 dots were counted on the model membrane, attributed to reduced impediments in incorporation and less local curvature stress of OA. After buffer rinsing, dark areas appeared, indicating defects on the model membrane. These defects suggest that the induced curved structures were washed away due to changes in surface tension in the affected regions. Following washing, only 388 ± 17 dots remained, a count higher than that observed with LipoLNA before rinsing, indicating that LipoOA induced more significant lipid bilayer component rearrangements. Similarly, exposure to 15.625 μg/mL of LipoOA resulted in a greater number of tiny bright spots compared to those observed with LipoLNA and LipoLLA at lower concentrations, indicating more extensive incorporation of LipoOA into the membrane. In comparison to higher concentrations, less membrane change was observed.

The incorporation of LCFAs into lipid bilayers induces diverse morphological changes by disrupting the lipid order within bacterial membranes. The insertion of these non-

https://doi.org/10.1021/acsami.5c00787
ACS Appl. Mater. Interfaces 2025, 17, 23666−23679

cylindrical molecules generates curvature stress and lateral pressure in the surrounding lipid environment, thereby altering the membrane's surface curvature and destabilizing its structural integrity.[64,66] This disruption is heavily influenced by the degree of unsaturation in the LCFA molecules. LCFAs with lower levels of unsaturation tend to induce flatter membrane morphologies due to reduced curvature stress, whereas highly unsaturated LCFAs generate more pronounced curvature stress, resulting in significant morphological changes such as large membrane buds or smaller, dense protrusions. For example, LNA, with a high degree of unsaturation, produces substantial curvature stress, leading to prominent budding, while OA, with fewer unsaturated bonds, causes more compact protrusions. These localized membrane deformations not only reflect the physical disruption of the lipid bilayer but also enhance interactions with liposomal formulations. Thus, the degree of unsaturation critically governs the extent and nature of these structural transformations, with greater unsaturation correlating to heightened curvature stress and more pronounced morphological effects.

***In Vitro* Membrane Fluidity Changes Induced by LipoLNA, LipoLLA, and LipoOA on Gram-Positive Bacterial Membranes.** The incorporation of cis-unsaturated FAs in bacterial membranes can affect the membrane fluidity by inducing rearrangements of surrounding lipid molecules, thus changing the membrane properties.[39,40,67] To evaluate these changes in membrane lipid behavior upon exposure to LipoFAs, FRAP measurements were conducted to measure the diffusion coefficient and mobile fraction of lipid molecules in the model membranes. As show in Figure 5A, BareLipo increased the lateral lipid diffusion (diffusion coefficient) within the model membrane by 35.2%, LipoLNA by 18.4%, while LipoLLA and LipoOA decreased it by 37.8% and 91.8%, respectively. Concurrently, the mobile fraction of the lipid molecules was 80.0 ± 3% for LipoLNA, 43.8 ± 0.8% for LipoLLA, and 25.7 ± 2.2% for LipoOA. The reduction in the diffusion coefficient suggests an increase in lipid molecule rearrangement to restore the membrane. Meantime, the disruption of membrane integrity will also reduce the diffusion coefficient and mobile fraction. A higher degree of unsaturation leads to a more irregular arrangement of lipid molecules, facilitating easier movement within the membrane. Conversely, the mobile fraction of the exposed membrane was calculated to reflect the membrane's recovery rate. LipoOA exhibited the lowest mobile fraction of 25.7 ± 2.2% with only a quarter of the destabilized membrane was restored, indicating less integrity of the membrane after exposed to LipoOA. In contrast, the presence of three unsaturated bonds in LipoLNA leads to a more disordered arrangement of lipid molecules in the membrane.[68]

To further substantiate the changes in membrane properties after treatment with LipoFAs, the fluidity of the bacterial membrane was assessed using Laurdan Generalized Polarization (GP) intensity (Figure 5F). The Laurdan GP values for membranes treated with LipoFAs were 0.457 ± 0.017 for LipoLNA, 0.471 ± 0.005 for LipoLLA, and 0.477 ± 0.006 for LipoOA, respectively. The results indicated that *S. aureus* MW2 treated with LipoFAs exhibited increased membrane rigidity, consistent with the observations from the FRAP results, suggesting that the incorporation of FAs into the membrane induced changes in fluidity.

***In Vitro* Antibacterial, Membrane Permeability, and ATP Leakage Assessments of *S. aureus* MW2.** To assess the antimicrobial activity of LipoFAs, a time-kill kinetic analysis was performed against methicillin-resistant *Staphylococcus aureus* (MRSA) strain MW2 (Figure 6A). LipoFAs showed a reduction in viability at 16 μg/mL. Notably, LipoLNA reduced viability by more than 2-log at 63 μg/mL and completely eradicated MRSA MW2 cells at 125 μg/mL. LipoLLA achieved a greater than 2-log reduction at 31 μg/mL and fully eliminated cells at 125 μg/mL. LipoOA showed a 1-log reduction in viability at 500 μg/mL.

Subsequently, we explored the impacts of LipoFAs on *S. aureus* MW2 membranes based on SYTOX Green permeability and intracellular ATP leakage. *S. aureus* treated with LipoLNA showed a concentration-dependent increase in relative fluorescence units (RFU) over time, with a particularly sharp rise at concentrations of 125 μg/mL or higher (Figure 6B), indicating a marked increase in membrane permeability. Similarly, LipoLLA treatment resulted in a substantial increase in permeability, with RFU notably rising at concentrations above 63 μg/mL. In contrast, LipoOA had a relatively lower impact on permeability, with less pronounced concentration-dependent changes compared to LipoLNA and LipoLLA owing to their differences in structure. LNA and LLA produce larger local stress on lipid membranes compared to OA with straighter tail. The BareLipo control group exhibited almost no change in permeability, indicating that the bacterial membranes remained stable in the absence of LCFAs.

LipoLNA also induced a concentration-dependent increase in ATP release, particularly significant at concentrations of 250 μg/mL and above (Figure 6C). The LipoLLA-treated group showed a similar trend, with significant ATP leakage at higher concentrations. In contrast, LipoOA caused relatively lower ATP leakage, with significant differences observed at concentrations of 63 μg/mL or higher. The BareLipo control group exhibited minimal ATP leakage, suggesting no membrane disruption in the absence of LCFAs. Treatment with LCFAs also led to ATP leakage in a concentration-dependent manner, though to a lesser extent than the LipoFAs. Overall, LipoFAs, particularly LipoLNA and LipoLLA, significantly disrupt membrane integrity. These results demonstrate that the unsaturated bond structures of these FAs significantly compromise bacterial membrane integrity. These findings demonstrate that unsaturated bond structures of LCFAs exert high local stress on the membrane, significantly compromising bacterial membrane integrity.

***In Vitro* Cytotoxicity Evaluation of the Prepared LipoFAs.** In addition to the solubility challenges associated with FAs, their inherent cytotoxicity represents a significant drawback that limits their application as antimicrobial agents. The cytotoxic effects of FAs have been well documented in numerous research investigations. Literature reports have linked FAs to cell toxicity through various pathways like apoptosis, autophagy, and disruption of cellular pathways.[69,70] This aspect hampers the utilization of FAs as antimicrobial agents, emphasizing the need to address this issue for further development of effective therapeutic strategies. To investigate the in vitro cytotoxic effects of FFAs and LipoFAs, mouse fibroblast cells (L-929) and human keratinocyte cells (HaCat) were employed as test models.

Subsequent cell viability assays were conducted on mouse fibroblast cells (L-929) and human keratinocyte cells (HaCat) (Figure 7A,B). FFAs began to exhibit cytotoxic effects at a concentration of 125 μg/mL in L-929 cells, reducing cell viability to approximately 80%. Conversely, LipoFAs main-

https://doi.org/10.1021/acsami.5c00787
ACS Appl. Mater. Interfaces 2025, 17, 23666−23679

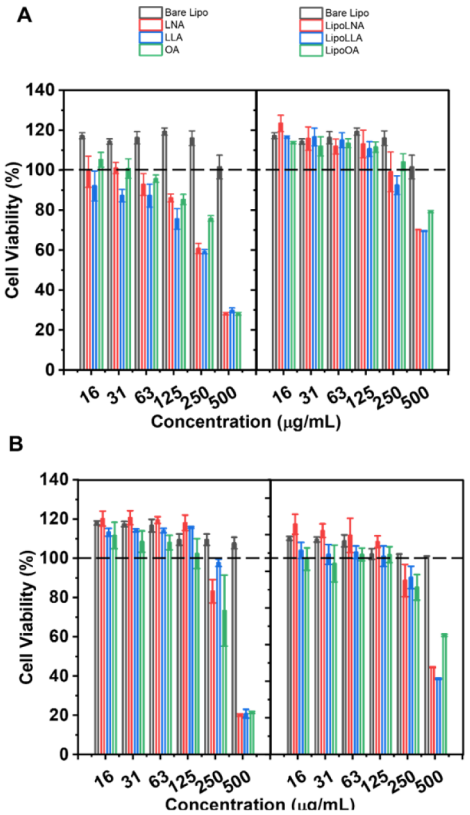

Figure 7. *In vitro* cell viability assays for *S. aureus* MW2 after treatment with LCFAs and LipoFAs. Cell viability analysis on (A) mouse fibroblast cells (L-929) and (B) human keratinocyte cells (HaCat) treated with LCFAs, BareLipos, and LipoFAs (n = 3, mean ± SD).

tained approximately 100% viability up to 125 μg/mL and over 90% viability at 250 μg/mL in both cell lines, indicating minimal toxicity. At 125 μg/mL, FFAs exhibited lower viability in L-929 cells, with cell viability values of 86.2% for free LNA, 75.7% for free LLA, and 85.4% for free OA. At higher concentrations, cytotoxicity increased, with viability dropping to 28.4% for free LNA, 30.1% for free LLA, and 28.4% for free OA at 500 μg/mL in L-929 cells. In HaCat cells, viability decreased to 20.3% for free LNA, 21.7% for free LLA, and 20.9% for free OA at 500 μg/mL. In contrast, LipoFAs significantly improved cell viability, with approximately 70% of L-929 cells and over 40% of HaCat cells surviving at 500 μg/mL. These results suggest that LipoFAs exhibit lower cytotoxicity at higher concentrations, supporting their potential as effective antibacterial agents with enhanced biocompatibility compared to FFAs.

CONCLUSIONS

This study presents a detailed analysis of the interaction patterns between LipoFAs and Gram-positive model membranes utilizing various biophysical and biological techniques. The research delves into how LipoFAs fuse and integrate with phospholipid membrane constituents, leading to modifications in the membrane's mass and viscoelastic attributes. The formulated LipoFA compositions with the optimal weight ratio exhibited a notable reduction in zeta potential of ∼ −50 mV and an intermediate size of ∼ 140 nm, indicating a propensity to fuse with Gram-positive model membranes. Biophysical experimental results revealed that a higher level of unsaturation in the FA tails hinders their integration and rearrangement within the Gram-positive model membrane, likely due to increased local curvature stress surrounding the FAs. In contrast, FAs with fewer unsaturated bonds are more easily incorporated and generate less curvature stress. Biological assessments demonstrated that liposomes loaded with LCFAs displaying higher unsaturation levels led to increase membrane fluidity, permeability, intracellular ATP leakage, and consequently, enhanced bactericidal effects on MRSA. Moreover, LipoFAs exhibited reduced cytotoxicity, highlighting their potential as effective antibacterial agents with enhanced biocompatibility compared to FFAs. These findings provide critical insights into the biophysical mechanisms underlying FA-membrane interactions, offering a platform for the rational design of next-generation antimicrobial agents. By elucidating the relationships between FA structure, membrane interaction, and bactericidal efficacy, this study lays the groundwork for developing tailored lipid-based therapeutics that leverage specific structural properties to target bacterial membranes more effectively. Future research should focus on evaluating the *in vivo* efficacy of LipoFAs to validate their therapeutic potential in clinical settings. Investigating the ability of LipoFAs to disrupt biofilms, which are clinically relevant for persistent infections, represents another critical avenue for advancing these formulations. Such research will be instrumental in addressing the global challenge of antibiotic resistance and guiding the development of robust, next-generation antimicrobial therapies.

ASSOCIATED CONTENT

Supporting Information

The Supporting Information is available free of charge at https://pubs.acs.org/doi/10.1021/acsami.5c00787.

QCM-D traces for LipoFAs on Gram-positive model membranes (PDF)

AUTHOR INFORMATION

Corresponding Author

Nam-Joon Cho − *School of Materials Science and Engineering, Nanyang Technological University, Singapore 639798, Singapore; Singapore-HUJ Alliance for Research and Enterprise, Singapore HUJ Alliance Research Enterprise (SHARE) 1 CREATE Way, Singapore 138602, Singapore; Centre for Cross Economy, Nanyang Technological University, Singapore 637551, Singapore;* orcid.org/0000-0002-8692-8955; Email: njcho@ntu.edu.sg

Authors

Sungmin Shin − *School of Materials Science and Engineering, Nanyang Technological University, Singapore 639798, Singapore; Singapore-HUJ Alliance for Research and Enterprise, Singapore HUJ Alliance Research Enterprise (SHARE) 1 CREATE Way, Singapore 138602, Singapore; Centre for Cross Economy, Nanyang Technological University, Singapore 637551, Singapore*

Dongping Jiang − *School of Materials Science and Engineering, Nanyang Technological University, Singapore 639798, Singapore; Singapore-HUJ Alliance for Research and Enterprise, Singapore HUJ Alliance Research Enterprise (SHARE) 1 CREATE Way, Singapore 138602, Singapore; Centre for Cross Economy, Nanyang Technological University, Singapore 637551, Singapore*

https://doi.org/10.1021/acsami.5c00787
ACS Appl. Mater. Interfaces 2025, 17, 23666−23679

Jingyeong Yu − *College of Pharmacy, Graduate School of Pharmaceutical Sciences, Ewha Womans University, Seoul 03760, Republic of Korea*
Chungmo Yang − *School of Materials Science and Engineering, Nanyang Technological University, Singapore 639798, Singapore*
Woncheol Jeong − *School of Materials Science and Engineering, Nanyang Technological University, Singapore 639798, Singapore; Centre for Cross Economy, Nanyang Technological University, Singapore 637551, Singapore*
Jian Li − *School of Materials Science and Engineering, Nanyang Technological University, Singapore 639798, Singapore; Centre for Cross Economy, Nanyang Technological University, Singapore 637551, Singapore*
Jieun Bae − *Department of Research and Development, LUCA AICell Inc, Anyang 14055, Republic of Korea*
Jihoon Shin − *School of Materials Science and Engineering, Nanyang Technological University, Singapore 639798, Singapore; Department of Research and Development, LUCA AICell Inc, Anyang 14055, Republic of Korea*
Kyongman An − *Department of Research and Development, LUCA AICell Inc, Anyang 14055, Republic of Korea;* Present Address: Department of Industrial AI Engineering, Graduate School of Management of Technology, Hoseo University, Asan, 31499, Republic of Korea; orcid.org/0000-0001-8393-6231
Wooseong Kim − *College of Pharmacy, Graduate School of Pharmaceutical Sciences, Ewha Womans University, Seoul 03760, Republic of Korea*

Complete contact information is available at: https://pubs.acs.org/10.1021/acsami.5c00787

Notes

The authors declare no competing financial interest.

■ ACKNOWLEDGMENTS

This work was supported by National Research Foundation of Korea (NRF) grants funded by the Ministry of Science and ICT (2021K1A4A7A0209781012, 2018R1A5A2025286) and by National Institute of Health (NIH) grants funded by the Korea Disease Control and Prevention Agency (KDCA) (2022ER240600). This work was also supported by the Ministry of Education (MOE) in Singapore under grants RG111/20 and RG34/22. This research was also supported by the National Research Foundation, Singapore, through its Campus for Research Excellence and Technological Enterprise (CREATE) Project Code: 37018451. In addition, this research was supported by the Ministry of Education (MOE) grant MOE-MOET32022-0002.

■ REFERENCES

(1) Fongang, H.; Mbaveng, A. T.; Kuete, V.; Chapter One - Global burden of bacterial infections and drug resistance. In *Advances in Botanical Research*. Kuete, V. Ed., Academic Press: 2023, Vol. *106*, pp. 1−20.
(2) Kwon, J. H.; Powderly, W. G. The post-antibiotic era is here. *Science* **2021**, *373* (6554), 471.
(3) Casillas-Vargas, G.; Ocasio-Malavé, C.; Medina, S.; Morales-Guzmán, C.; Del Valle, R. G.; Carballeira, N. M.; Sanabria-Ríos, D. J. Antibacterial fatty acids: An update of possible mechanisms of action and implications in the development of the next-generation of antibacterial agents. *Prog. Lipid Res.* **2021**, *82*, 101093.
(4) Desbois, A. P.; Smith, V. J. Antibacterial free fatty acids: Activities, mechanisms of action and biotechnological potential. *Appl. Microbiol. Biotechnol.* **2010**, *85* (6), 1629−1642.
(5) Yoon, B. K.; Jackman, J. A.; Valle-González, E. R.; Cho, N.-J. Antibacterial free fatty acids and monoglycerides: Biological activities, experimental testing, and therapeutic applications. *Int. J. Mol. Sci.* **2018**, *19* (4), 1114.
(6) Yoon, B. K.; Jackman, J. A.; Kim, M. C.; Cho, N.-J. Spectrum of membrane morphological responses to antibacterial fatty acids and related surfactants. *Langmuir* **2015**, *31* (37), 10223−10232.
(7) Hagve, T.-A. Effects of unsaturated fatty acids on cell membrane functions. *Scand. J. Clin. Lab. Invest.* **1988**, *48* (5), 381−388.
(8) Galbraith, H.; Miller, T. B.; Paton, A. M.; Thompson, J. K. Antibacterial Activity of Long Chain Fatty Acids and the Reversal with Calcium, Magnesium, Ergocalciferol and Cholesterol. *J. Appl. Bacteriol.* **1971**, *34* (4), 803−813.
(9) Kabara, J. J.; Vrable, R.; Lie Ken Jie, M. S. F. Antimicrobial lipids: Natural and synthetic fatty acids and monoglycerides. *Lipids* **1977**, *12* (9), 753−759.
(10) Lee, J. Y.; Kim, Y. S.; Shin, D. H. Antimicrobial synergistic effect of linolenic acid and monoglyceride against Bacillus cereus and Staphylococcus aureus. *J. Agric. Food Chem.* **2002**, *50* (7), 2193−2199.
(11) Desbois, A. P.; Lawlor, K. C. Antibacterial activity of long-chain polyunsaturated fatty acids against Propionibacterium acnes and Staphylococcus aureus. *Mar. Drugs* **2013**, *11* (11), 4544−4557.
(12) Yuyama, K. T.; Rohde, M.; Molinari, G.; Stadler, M.; Abraham, W.-R. Unsaturated Fatty Acids Control Biofilm Formation of Staphylococcus aureus and Other Gram-Positive Bacteria. *Antibiotics* **2020**, *9* (11), 788.
(13) Zheng, C. J.; Yoo, J.-S.; Lee, T.-G.; Cho, H.-Y.; Kim, Y.-H.; Kim, W.-G. Fatty acid synthesis is a target for antibacterial activity of unsaturated fatty acids. *FEBS Lett.* **2005**, *579* (23), 5157−5162.
(14) Kenar, J. A.; Moser, B. R.; List, G. R. Chapter 2 - Naturally Occurring Fatty Acids: Source, Chemistry, and Uses. In *Fatty Acids: Chemistry, Synthesis, and Applications*, Ahmad, M. U., Ed.; AOCS Press: 2017, pp. 23−82.
(15) Kinsella, J. E. Grapeseed oil: A rich source of linoleic acid. *Food Technol.* **1974**, *28* (5), 58−60.
(16) DeBonte, L.; Iassonova, D.; Liu, L.; Loh, W. Commercialization of high oleic canola oils. *Lipid Technol.* **2012**, *24* (8), 175−177.
(17) Tan, J. Y. B.; Yoon, B. K.; Cho, N.-J.; Lovrić, J.; Jug, M.; Jackman, J. A. Lipid Nanoparticle Technology for Delivering Biologically Active Fatty Acids and Monoglycerides. *Int. J. Mol. Sci.* **2021**, *22* (18), 9664.
(18) Holman, R. T.; Elmer, O. C. The rates of oxidation of unsaturated fatty acids and esters. *J. Am. Oil Chem. Soc.* **1947**, *24* (4), 127−129.
(19) Schulz, H. Chapter 5 Oxidation of fatty acids in eukaryotes. *New Compr. Biochem.* **2002**, *36*, 127−150.
(20) Fu, X.; Feng, F.; Huang, B. Physicochemical characterization and evaluation of a microemulsion system for antimicrobial activity of glycerol monolaurate. *Int. J. Pharm.* **2006**, *321* (1), 171−175.
(21) Üstündag-Okur, N.; Gökçe, E. H.; Egrilmez, S.; Özer, Ö.; Ertan, G. Novel ofloxacin-loaded microemulsion formulations for ocular delivery. *J. Ocul. Pharmacol. Ther.* **2014**, *30* (4), 319−332.
(22) Vélez, M. A.; Perotti, M. C.; Hynes, E. R.; Gennaro, A. M. Effect of lyophilization on food grade liposomes loaded with conjugated linoleic acid. *J. Food Eng.* **2019**, *240*, 199−206.
(23) Pushparaj Selvadoss, P.; Nellore, J.; Balaraman Ravindrran, M.; Sekar, U.; Tippabathani, J. Enhancement of antimicrobial activity by liposomal oleic acid-loaded antibiotics for the treatment of multidrug-resistant Pseudomonas aeruginosa. *Artif. Cells, Nanomed., Biotechnol.* **2018**, *46* (2), 268−273.
(24) Yan, L.; Wang, L.; Gao, S.; Liu, C.; Zhang, Z.; Ma, A.; Zheng, L. Celery cellulose hydrogel as carriers for controlled release of short-chain fatty acid by ultrasound. *Food Chem.* **2020**, *309*, 125717.
(25) Mei, L.; Zhang, D.; Shao, H.; Hao, Y.; Zhang, T.; Zheng, W.; Ji, Y.; Ling, P.; Lu, Y.; Zhou, Q. Injectable and Self-Healing Probiotics-

Loaded Hydrogel for Promoting Superbacteria-Infected Wound Healing. *ACS Appl. Mater. Interfaces* **2022**, *14* (18), 20538−20550.
(26) Butt, U.; ElShaer, A.; Snyder, L. A. S.; Al-Kinani, A. A.; Le Gresley, A.; Alany, R. G. Fatty Acid Based Microemulsions to Combat Ophthalmia Neonatorum Caused by Neisseria gonorrhoeae and Staphylococcus aureus. *Nanomaterials* **2018**, *8* (1), 51.
(27) Torres-Luna, C.; Hu, N.; Fan, X.; Domszy, R.; Yang, J.; Briber, R. M.; Yang, A. Extended delivery of cationic drugs from contact lenses loaded with unsaturated fatty acids. *Eur. J. Pharm. Biopharm.* **2020**, *155*, 1−11.
(28) Zhang, L.; Pornpattananangkul, D.; Hu, C.-M.; Huang, C.-M. Development of nanoparticles for antimicrobial drug delivery. *Curr. Med. Chem.* **2010**, *17* (6), 585−594.
(29) Huang, C. M.; Chen, C. H.; Pornpattananangkul, D.; Zhang, L.; Chan, M.; Hsieh, M. F.; Zhang, L. Eradication of drug resistant Staphylococcus aureus by liposomal oleic acids. *Biomaterials* **2011**, *32* (1), 214−221.
(30) Lieb, L. M.; Ramachandran, C.; Egbaria, K.; Weiner, N. Topical delivery enhancement with multilamellar liposomes into pilosebaceous units: I. In vitro evaluation using fluorescent techniques with the hamster ear model. *J. Invest. Dermatol.* **1992**, *99* (1), 108−113.
(31) Torchilin, V. P. Recent advances with liposomes as pharmaceutical carriers. *Nat. Rev. Drug Discovery* **2005**, *4* (2), 145−160.
(32) Jung, S. W.; Thamphiwatana, S.; Zhang, L.; Obonyo, M. Mechanism of antibacterial activity of liposomal linolenic acid against Helicobacter pylori. *PLoS One* **2015**, *10* (3), No. e0116519.
(33) Halverson, L. J.; Firestone, M. K. Differential effects of permeating and nonpermeating solutes on the fatty acid composition of Pseudomonas putida. *Appl. Environ. Microbiol.* **2000**, *66* (6), 2414−2421.
(34) Ge, X.; Shi, X.; Shi, L.; Liu, J.; Stone, V.; Kong, F.; Kitten, T.; Xu, P. Involvement of NADH Oxidase in Biofilm Formation in Streptococcus sanguinis. *PLoS One* **2016**, *11* (3), No. e0151142.
(35) Itoh, T.; Takenawa, T. Mechanisms of membrane deformation by lipid-binding domains. *Prog. Lipid Res.* **2009**, *48* (5), 298−305.
(36) Gohrbandt, M.; Lipski, A.; Grimshaw, J. W.; Buttress, J. A.; Baig, Z.; Herkenhoff, B.; Walter, S.; Kurre, R.; Deckers-Hebestreit, G.; Strahl, H. Low membrane fluidity triggers lipid phase separation and protein segregation in living bacteria. *EMBO J.* **2022**, *41* (5), No. e109800.
(37) Or, D.; Smets, B. F.; Wraith, J. M.; Dechesne, A.; Friedman, S. P. Physical constraints affecting bacterial habitats and activity in unsaturated porous media − a review. *Adv. Water Resour.* **2007**, *30* (6), 1505−1527.
(38) Obonyo, M.; Zhang, L.; Thamphiwatana, S.; Pornpattananangkul, D.; Fu, V.; Zhang, L. Antibacterial Activities of Liposomal Linolenic Acids against Antibiotic-Resistant Helicobacter pylori. *Mol. Pharmaceutics* **2012**, *9* (9), 2677−2685.
(39) Greenway, D. L.; Dyke, K. G. Mechanism of the inhibitory action of linoleic acid on the growth of Staphylococcus aureus. *J. Gen. Microbiol.* **1979**, *115* (1), 233−245.
(40) Chamberlain, N. R.; Mehrtens, B. G.; Xiong, Z.; Kapral, F. A.; Boardman, J. L.; Rearick, J. I. Correlation of carotenoid production, decreased membrane fluidity, and resistance to oleic acid killing in Staphylococcus aureus 18Z. *Infect. Immun.* **1991**, *59* (12), 4332−4337.
(41) Murínová, S.; Dercová, K.; Čertík, M.; Lászlová, K. The adaptation responses of bacterial cytoplasmic membrane fluidity in the presence of environmental stress factors — polychlorinated biphenyls and 3-chlorobenzoic acid. *Biologia* **2014**, *69* (4), 428−434.
(42) Yang, D.; Pornpattananangkul, D.; Nakatsuji, T.; Chan, M.; Carson, D.; Huang, C. M.; Zhang, L. The antimicrobial activity of liposomal lauric acids against Propionibacterium acnes. *Biomaterials* **2009**, *30* (30), 6035−6040.
(43) Mayer, L. D.; Hope, M. J.; Cullis, P. R. Vesicles of variable sizes produced by a rapid extrusion procedure. *Biochim. Biophys. Acta, Protein Struct. Mol. Enzymol.* **1986**, *858* (1), 161−168.
(44) Shin, S.; Yu, J.; Tae, H.; Zhao, Y.; Jiang, D.; Qiao, Y.; Kim, W.; Cho, N.-J. Exploring the Membrane-Active Interactions of Antimicrobial Long-Chain Fatty Acids Using a Supported Lipid Bilayer Model for Gram-Positive Bacterial Membranes. *ACS Appl. Mater. Interfaces* **2024**, *16* (42), 56705−56717.
(45) Tabaei, S. R.; Choi, J. H.; Haw Zan, G.; Zhdanov, V. P.; Cho, N. J. Solvent-assisted lipid bilayer formation on silicon dioxide and gold. *Langmuir* **2014**, *30* (34), 10363−10373.
(46) Di Leone, S.; Kyropoulou, M.; Köchlin, J.; Wehr, R.; Meier, W. P.; Palivan, C. G. Tailoring a Solvent-Assisted Method for Solid-Supported Hybrid Lipid−Polymer Membranes. *Langmuir* **2022**, *38* (21), 6561−6570.
(47) Dixon, M. C. Quartz crystal microbalance with dissipation monitoring: Enabling real-time characterization of biological materials and their interactions. *J. Biomol. Technol.* **2008**, *19* (3), 151−158.
(48) Jönsson, P.; Jonsson, M. P.; Tegenfeldt, J. O.; Höök, F. A method improving the accuracy of fluorescence recovery after photobleaching analysis. *Biophys. J.* **2008**, *95* (11), 5334−5348.
(49) Mouritsen, O. G. Lipids, curvature, and nano-medicine. *Eur. J. Lipid Sci. Technol.* **2011**, *113* (10), 1174−1187.
(50) Danaei, M.; Dehghankhold, M.; Ataei, S.; Hasanzadeh Davarani, F.; Javanmard, R.; Dokhani, A.; Khorasani, S.; Mozafari, M. R. Impact of Particle Size and Polydispersity Index on the Clinical Applications of Lipidic Nanocarrier Systems. *Pharmaceutics* **2018**, *10* (2), 57.
(51) Dejeu, I. L.; Vicas, L. G.; Jurca, T.; Teusdea, A. C.; Muręan, M. E.; Fritea, L.; Svera, P.; Gabor, G. A.; Dejeu, G. E.; Maghiar, O. A.; et al. Liposomes with Caffeic Acid: Morphological and Structural Characterisation, Their Properties and Stability in Time. *Processes* **2021**, *9* (6), 912.
(52) Ramli, N. A.; Ali, N. A.; Hamzah, S. Physicochemical Characterization of Quercetin-Loaded Liposomes Prepared by Sonication for Functional Food Application. *J. Sustainability Sci. Manage.* **2020**, *15* (6), 15−27.
(53) Li, R.; Zhang, L. Y.; Li, Z. J.; Xue, C. H.; Dong, P.; Huang, Q. R.; Wang, Y. M.; Zhang, T. T. Characterization and Absorption Kinetics of a Novel Multifunctional Nanoliposome Stabilized by Sea Cucumber Saponins Instead of Cholesterol. *J. Agric. Food Chem.* **2020**, *68* (2), 642−651.
(54) Thamphiwatana, S.; Gao, W.; Obonyo, M.; Zhang, L. In vivo treatment of *Helicobacter pylori* infection with liposomal linolenic acid reduces colonization and ameliorates inflammation. *Proc. Int. Acad. Sci.* **2014**, *111* (49), 17600−17605.
(55) Dragicevic-Curic, N.; Gräfe, S.; Gitter, B.; Winter, S.; Fahr, A. Surface charged temoporfin-loaded flexible vesicles: In vitro skin penetration studies and stability. *Int. J. Pharm.* **2010**, *384* (1), 100−108.
(56) Dragicevic-Curic, N.; Winter, S.; Krajisnik, D.; Stupar, M.; Milic, J.; Graefe, S.; Fahr, A. Stability evaluation of temoporfin-loaded liposomal gels for topical application. *J. Liposome Res.* **2010**, *20* (1), 38−48.
(57) Peretz Damari, S.; Shamrakov, D.; Varenik, M.; Koren, E.; Nativ-Roth, E.; Barenholz, Y.; Regev, O. Practical aspects in size and morphology characterization of drug-loaded nano-liposomes. *Int. J. Pharm.* **2018**, *547* (1), 648−655.
(58) Hasan, I. Y.; Mechler, A. Viscoelastic changes measured in partially suspended single bilayer membranes. *Soft Matter* **2015**, *11* (27), 5571−5579.
(59) Seantier, B.; Breffa, C.; Félix, O.; Decher, G. Dissipation-Enhanced Quartz Crystal Microbalance Studies on the Experimental Parameters Controlling the Formation of Supported Lipid Bilayers. *J. Phys. Chem. B* **2005**, *109* (46), 21755−21765.
(60) Flynn, K. R.; Martin, L. L.; Ackland, M. L.; Torriero, A. A. J. Real-Time Quartz Crystal Microbalance Monitoring of Free Docosahexaenoic Acid Interactions with Supported Lipid Bilayers. *Langmuir* **2016**, *32* (45), 11717−11727.
(61) Asai, N.; Matsumoto, N.; Yamashita, I.; Shimizu, T.; Shingubara, S.; Ito, T. Detailed analysis of liposome adsorption and

its rupture on the liquid-solid interface monitored by LSPR and QCM-D integrated sensor. *Sens. Bio-Sens. Res.* **2021**, *32*, 100415.
(62) Koyanagi, T.; Cao, K. J.; Leriche, G.; Onofrei, D.; Holland, G. P.; Mayer, M.; Sept, D.; Yang, J. Hybrid Lipids Inspired by Extremophiles and Eukaryotes Afford Serum-Stable Membranes with Low Leakage. *Chem. - Eur. J.* **2017**, *23* (28), 6757−6762.
(63) Walker, L. R.; Marty, M. T. Lipid tails modulate antimicrobial peptide membrane incorporation and activity. *Biochim. Biophys. Acta, Biomembr.* **2022**, *1864* (4), 183870.
(64) Arouri, A.; Mouritsen, O. G. Membrane-perturbing effect of fatty acids and lysolipids. *Prog. Lipid Res.* **2013**, *52* (1), 130−140.
(65) Thid, D.; Benkoski, J. J.; Svedhem, S.; Kasemo, B.; Gold, J. DHA-Induced Changes of Supported Lipid Membrane Morphology. *Langmuir* **2007**, *23* (11), 5878−5881.
(66) Jespersen, H.; Andersen, J. H.; Ditzel, H. J.; Mouritsen, O. G. Lipids, curvature stress, and the action of lipid prodrugs: Free fatty acids and lysolipid enhancement of drug transport across liposomal membranes. *Biochimie* **2012**, *94* (1), 2−10.
(67) Lopez, M. S.; Tan, I. S.; Yan, D.; Kang, J.; McCreary, M.; Modrusan, Z.; Austin, C. D.; Xu, M.; Brown, E. J. Host-derived fatty acids activate type VII secretion in *Staphylococcus aureus*. *Proc. Int. Acad. Sci.* **2017**, *114* (42), 11223−11228.
(68) Ibarguren, M.; López, D. J.; Escribá, P. V. The effect of natural and synthetic fatty acids on membrane structure, microdomain organization, cellular functions and human health. *Biochim. Biophys. Acta, Biomembr.* **2014**, *1838* (6), 1518−1528.
(69) Sun, S.; Li, M.; Dong, F.; Wang, S.; Tian, L.; Mann, S. Chemical Signaling and Functional Activation in Colloidosome-Based Protocells. *Small* **2016**, *12* (14), 1920−1927.
(70) Engelbrecht, A. M.; Toit-Kohn, J.-L. D.; Ellis, B.; Thomas, M.; Nell, T.; Smith, R. Differential Induction of Apoptosis and Inhibition of the PI3-kinase Pathway by Saturated, Monounsaturated and Polyunsaturated Fatty Acids in a Colon Cancer Cell Model. *Apoptosis* **2008**, *13* (11), 1368−1377.

https://doi.org/10.1021/acsami.5c00787
ACS Appl. Mater. Interfaces 2025, 17, 23666−23679